Journal of Electronic Materials (2025) 54:451–461
https://doi.org/10.1007/s11664-024-11535-6

ORIGINAL RESEARCH ARTICLE

Tailoring the Electrochemical Properties of ZnS Electrodes via Cobalt Doping for Improved Supercapacitor Application

Emmanuel Tom[1] · Abhijai Velluva[1,2,5] · Anit Joseph[2] · Tiju Thomas[2] · Mizaj Shabil Sha[3,4] · P. V Jithin[1] · Deepu Thomas[1] · Kishor Kumar Sadasivuni[3,4] · Joji Kurian[1]

Received: 30 November 2023 / Accepted: 4 October 2024 / Published online: 1 November 2024

Abstract
For practical uses, there has been a lot of interest in simple, inexpensive, and efficient synthesis of materials for supercapacitor applications. Pure and cobalt-doped zinc sulfide (Co-doped ZnS) powder samples were synthesized in this study using a straightforward co-precipitation process, and their electrochemical performance was examined. It was observed that, at a scan rate of 10 mV s^{-1}, pure ZnS has a specific capacitance of only 460.7 F g^{-1}; however, the Co-doping in ZnS increases it to 947.8 F g^{-1} for the 5% Co-doped sample, Co (0.05): ZnS. The results suggest that Co-doping in ZnS increases the kinetics and rate of redox processes. The increase in electrochemical active sites brought about by integrating Co into ZnS increases the surface area and results in the sample's capacity for storage. The encouraging findings increase the likelihood of elemental doping with other transition metal elements to increase the energy storage capability of earth-abundant ZnS samples.

Keywords Co-doped · ZnS · supercapacitor · capacitance

Introduction

Due to ever-growing energy demand and the increase in the global population, electrical energy storage systems are immensely needful for the present society. Even with renewable energy sources, which are not fully reliable, and other intermittent green energy sources, efficient and long-life energy storage systems are necessary to tackle the problem. Supercapacitors (SCs), also known as electrochemical capacitors, use a type of energy storage technology ideal for green and sustainable future, with their advantages being rapid charge–discharge (< 1 s to > 10 s), high power density (10,000 W kg^{-1}), sufficient energy density (~90 Wh kg^{-1}), high capacitance (few hundred to few thousand farads), long lifespan (~ 10^5 cycles), higher energy efficiency (~ 100%), and environmental friendliness.[1–5] Due to these favorable properties, SCs are useful in various applications, such as power grids, portable electronics, medical devices, aerospace appliances, telecommunication devices, and electric vehicles.[1,2,6,7] Supercapacitors outperform batteries and regular capacitors in terms of both specific power and cycle life. Nonetheless, conventional supercapacitors can only store energy without harvesting energy, and their energy density remains low when compared to batteries.[8] As a result, combining high specific energy and high specific power, long cycle life, and even quick self-charging in a single cell has been a potential approach for future energy storage technologies. Recently, multifunctional hybrid supercapacitors, such as asymmetric supercapacitors, batteries/supercapacitor hybrid devices, and self-charging hybrid supercapacitors, have received a lot of attention.[9]

SCs can be divided into two categories: (1) pseudocapacitors and (2) electric double-layer capacitors (EDLC). In the case of pseudocapacitors, the charge storage occurs through

✉ Kishor Kumar Sadasivuni
kishor_kumars@yahoo.com

✉ Joji Kurian
jojikuriank@gmail.com

1 Department of Physics, Nirmalagiri College (Kannur University), Nirmalagiri P. O, Kannur, Kerala 670701, India

2 Department of Metallurgical and Materials Engineering, Indian Institute of Technology Madras, Chennai, Tamil Nadu 600036, India

3 Center for Advanced Materials, Qatar University, PO Box 2713, Doha, Qatar

4 Department of Mechanical and Industrial Engineering, Qatar University, PO Box 2713, Doha, Qatar

5 Catalysis and Inorganic Chemistry Division, CSIR - National Chemical Laboratory, Pune 411008, India

rapid redox reactions based on faradaic charge transfer. In EDLCs, the storage mechanism is an electric double-layer formation of non-faradaic charges at the electrode-electrolyte interface via adsorption–desorption. Carbonaceous materials, such as graphene, carbon nanotubes, etc., are used as EDLCs because of their porous structure and high specific surface area.[10,11] EDLC faces limited energy density (10–20 Wh kg^{-1}) and specific capacitance (100–500 F g^{-1}).[12–15] Materials used for pseudo-capacitors include conducting polymers and transition metal compounds, such as oxides, nitrides, oxynitrides, sulfides, carbides, chalcogenides, etc.[10,16–23] Pseudo-capacitors have higher capacitance (10-100 times greater than that of EDLC), and energy density (20–80 Wh kg^{-1}) than EDLC but also have disadvantages, including lower power density (due to the slow nature of the faradaic process compared to non-faradaic), bad electrical conductivity (0.1–1 S m^{-1}), and limited cycle life (several hundred to thousand cycles).[11,24] Transition metal compounds are advantageous for electrochemical research due to their earth-abundant nature, low cost, distinctive physical and chemical features, and high specific capacitance.[25]

Transition metal sulfides are reported to have better electrochemical behavior (more than quintuple improvement in charge storage capacity) and high electrical conductivity compared to their metal oxide counterparts.[22,26] Since sulfur's electronegativity (2.58) is lesser than oxygen's (3.44), it may lead to a more flexible structure.[22] Zinc sulfide (ZnS) nanostructures are commonly studied because of their suitability to be used in a wide range of industrial applications and their properties, such as the ability to tune the bandgap (3.6–3.8 eV) with suitable dopants, excellent optical properties, low cost, ease of synthesis, and environmental friendliness. ZnS also shows excellent electrochemical properties, but further research is required to understand its potential. High capacity and excellent redox reversibility make it suitable in Li-ion batteries and SCs.[22]

In a single hydrothermal step, Hussain et al. created thin ZnS nanoflakes grown on nickel form (NF) and measured a specific capacity of 659 C g^{-1} at a current density of 2 A g^{-1} with high cycling stability. Hussain and colleagues evaluated the performance of Mn-doped ZnS with other nanostructures produced directly on NF in a different investigation.[27] Mn-doped nanoneedles, nanoflakes, and nanosheets have specific capacitances of 1517, 850, and 1905 F g^{-1}, respectively, at 1 A g^{-1}. Mn-doped ZnS nanosheets displayed the best performance with high capacitance retention.[12,22] For high-performance SCs, Yi et al. reported uniform-sized ZnS nanoparticles with a specific capacitance of 824 F g^{-1} at 1 A g^{-1}.[26] Additionally, the performance of supercapacitors was enhanced by the heterostructure of ZnS with other transition metal compounds and carbon compounds.[7,28–30] ZnS nanowires were deposited on NF using a single hydrothermal process, according to Rauf et al.,[31] and showed a specific capacitance of 781 F g^{-1} at 0.5 A g^{-1} and long-term cyclic stability. Ali et al. created a honeycomb-like structure of Mo-doped ZnS that was directly deposited on NF and demonstrated a high specific capacitance of 2208 F g^{-1} at 1 A g^{-1} in another investigation.[32] Ni-doped ZnS microspheres showed increased specific capacitance compared to pure ZnS microspheres, according to Rose et al.[33]

Doping and heterostructure are the two most utilized techniques to improve the electrochemical performance of materials by enhancing conductivity and introducing a synergistic effect. The cobalt doping in ZnS (Co-doped ZnS) improves its optical, electrical, magnetic, and photocatalytic properties.[34,35] Co^{2+} and Zn^{2+} have comparable ionic radii (58 pm and 60 pm) which will help to enhance the ZnS properties and both have a co-ordination number of 4.[35] The electrochemical performance of Co-doped ZnS has not been studied sufficiently. In this work, we have tried to improve the electrochemical performance of ZnS nanoparticles via cobalt doping. The Co-doped ZnS was synthesized through a simple chemical co-precipitation method, an industrially favorable low-cost technique.[36] The doping percentage of cobalt was varied at 1% and 5% to understand its doping effect in electrochemical performance. The as-synthesized doped and undoped samples were coated on NF and investigated for their electrochemical performances using a three-electrode working system.

Experimental

Materials and Chemicals

The precursor chemicals used for the synthesis of the samples includes zinc acetate [$Zn(CH_3COO)_2.2H_2O$], sodium sulfide (Na_2S), cobalt nitrate, [$Co(NO_3)_2.6H_2O$], potassium hydroxide (KOH), acetylene black (Sigma Aldrich), polyvinylidene fluoride (PVDF; Sigma Aldrich), and hydrochloric acid (HCl). Ni foam (99.9% pure, pore size: 0.05–0.5 mm) was procured from Nanoshel, Intelligent Material. Deionized water was used for washing.

Synthesis of pure ZnS and doped ZnS

Pure and transition metal-doped ZnS nanoparticles were synthesized at room temperature using a simple chemical co-precipitation technique. None of the chemicals employed in the synthesis underwent purification prior to usage. This procedure produced separate solutions of 0.2 M sodium sulfide and 0.2 M zinc acetate in 100 mL of deionized water. The sodium sulfide solution was added dropwise into the zinc acetate solution, causing the quick production of a white fluid, suggesting ZnS precipitation. This process does not use a capping agent, which may alter the particle

size, purity, and overall yield. The reaction mixture was then centrifuged to separate the white ZnS residue. To eliminate unreacted chemicals and contaminants, the solid product was centrifuged several times and rinsed with deionized water. Following purification, the precipitate was dried in an oven at 80°C for around 16 h. After drying, the material was ground into a fine powder and kept in a desiccator to avoid moisture absorption. Despite the method's simplicity, the lack of a capping agent and reagent purification may affect the final attributes of the ZnS product, such as particle size distribution and purity:

$$Zn(CH_3COO)_2 + Na_2S \rightarrow ZnS + 2NaCH_3COO \quad (1)$$

A chemical co-precipitation approach was used to synthesize cobalt-doped ZnS nanoparticles at various concentrations (1% and 5%). The technique began with the preparation of 0.2 M sodium sulfide and 0.2 M zinc acetate solutions, analogous to the production of pure ZnS. $Co(NO_3)_2{\cdot}6H_2O$ was added dropwise to the zinc acetate solution before introducing sodium sulfide. This regulated addition ensured a uniform distribution of cobalt ions throughout the ZnS matrix. The cobalt-doped ZnS nanoparticles were generated with two distinct doping concentrations, 1% and 5%, by varying the amount of cobalt nitrate used. The interaction between zinc acetate, sodium sulfide, and cobalt nitrate produced Co-doped ZnS nanoparticles. Following the reaction, the same processes as in the synthesis of pure ZnS were used, including centrifugation to collect the precipitate, several washings with deionized water to eliminate impurities, and drying in an oven at 80c for around 16 h. This technique resulted in Co-doped ZnS nanoparticles, with the cobalt doping concentration possibly influencing the material's optical, electrical, and structural properties:

$$\begin{aligned}&(1-x)Zn(CH_3COO)_2 + Na_2S + xCo(NO_3)_2\\&\rightarrow Zn_{1-x}Co_xS + 2NaCH_3COO + 2xNaNO_3\end{aligned} \quad (2)$$

Physical Characterization

The crystal structure and phase evaluation of all the synthesized samples were analyzed using x-ray diffraction (XRD; Rigaku) operated at 60 kV using Cu- K_α (1.5418 Å). The porous nature and specific surface area of samples were determined by performing the Brunauer–Emmett–Teller (BET; TB440A; Altamira) technique at 77.35 K after degassing the samples at 200°C for 3 h.

Electrochemical Characterization

The electrochemical performance of the samples was analyzed using 3-electrode measurements carried out in a CHI608E electrochemical workstation. In the 3-electrode setup, a platinum (Pt) mesh was used as the counter electrode, a saturated calomel electrode was used as the reference electrode, catalyst-coated NF was used as the working electrode, and 3 M KOH as the electrolyte. The slurry was prepared by mixing the active material (85 wt%), carbon black (10 wt%), and PVDF (5 wt%) in N-methyl-2 -pyrrolidone and ground well for 45 min. Before coating the slurry onto the porous NF, the NF was washed ultrasonically with 3 M HCl for 15 min to remove the oxide layers on the surface, followed by ethanol and distilled water for 10 min. The washed NF was dried in a hot-air oven for 6 h at 60°C, and the produced slurry was coated over the 1 × 1-cm^2 patch of cleaned NF using the brush-coating technique. After that, the coated electrode was dried for 6 h at 80°C. The constructed working electrode's active material mass loading ranged from 1.2 to 2.5 mg cm^{-2}. All the samples were subjected to electrochemical impedance spectroscopy (EIS) analyses with an AC amplitude of 5 mV at the open-circuit potential value, and the frequency range was 100 kHz to 100 mHz. Figure 6 shows the Nyquist plots with fitting curves for the pure and doped ZnS samples.

Results and Discussion

Material Characterization

The crystal structure of pure the ZnS and Co-doped ZnS samples were analyzed using the XRD characterization technique. Figure 1 shows the XRD patterns of the doped and pure samples, and the XRD pattern of pure ZnS is in good agreement and matches the standard data card (JCPDS No. 01-080-0020). The three major diffraction peaks at the 2θ values of 28.91°, 48.11°, and 58.12° indicate the (hkl) planes (111), (220), and (311), respectively, matching the synthesized sample. The XRD patterns of the doped ZnS samples, Co (0.01):ZnS and Co (0.05):ZnS, show an almost similar pattern to pure ZnS because of uniform doping and lower Co dopant content.[32,37–39] This also confirmed the development of a ZnS:Co^{2+} solid solution rather than Co precipitation or second phase. Furthermore, the doped ZnS nanocrystals' diffraction peaks shifted somewhat towards a high angle compared to the undoped ZnS nanocrystals, showing that cobalt ions have replaced zinc ions, resulting in lower lattice constants.[40–42]

The crystallite size of all the samples was calculated using the Scherrer formula:

$$D = \frac{k\lambda}{\beta cos\theta} \quad (3)$$

where D is the crystallite size, k is the shape factor, λ is the X-ray wavelength, β is full width at half-maximum (in

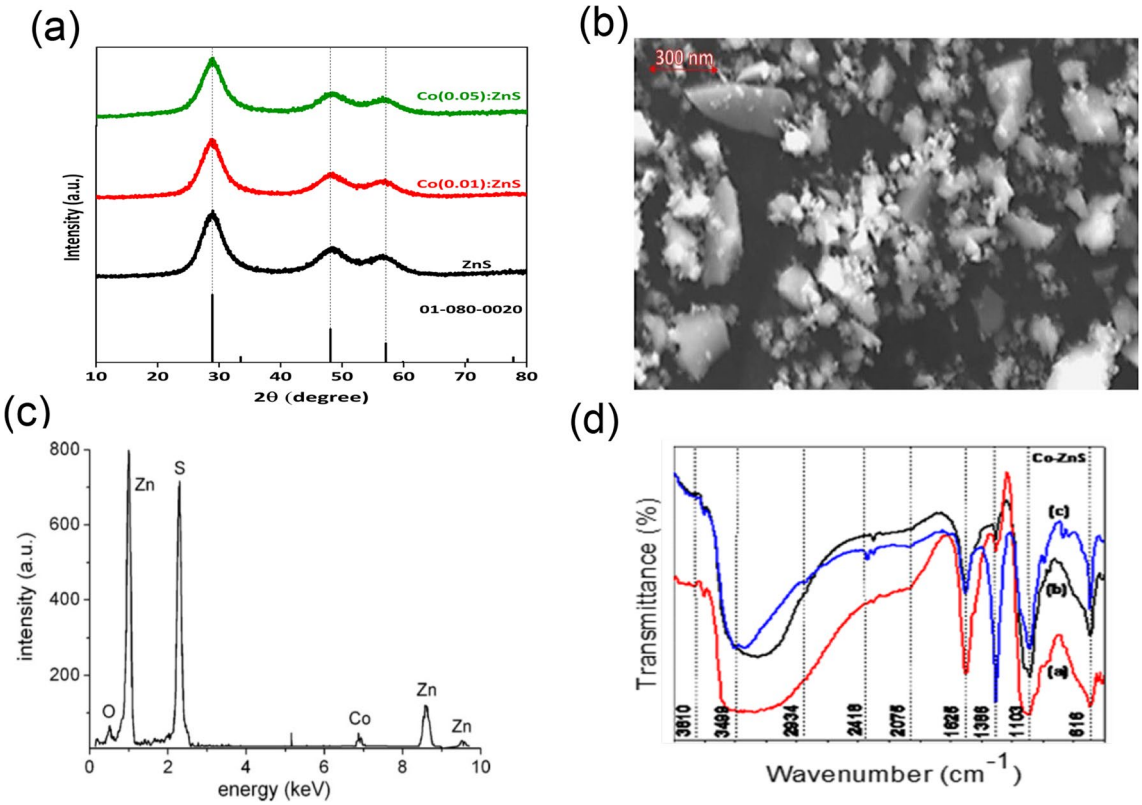

Fig. 1 (a) Powder XRD patterns of pure and Co-doped ZnS samples, (b) SEM micrographs of Co-doped ZnS sample, (c) EDX spectra of Co (0.01):ZnS, (d) FTIR spectra of Co-doped ZnS [*a* Co (0.01):ZnS, *b* Co (0.03):ZnS, *c* Co (0.05):ZnS)].

radians) of the diffraction peak, and θ is the corresponding diffraction angle (in degrees). Despite increasing the doping percentage of Co in ZnS, the crystallite size of the sample remained constant. The average crystallite size calculated using the Scherrer formula from high-intensity peaks for all the samples was ~ 1.87 nm. The size constancy is due to the low temperature of the heat treatment used, which does not lead to grain growth. This similarity of the peak profile is also suggestive of the Co ions being incorporated into the host matrix in place of the Zn sites.[43] The supplementary Table S1 contains in-depth research from the XRD spectrum.

The SEM micrograph of Co-doped ZnS NPs is shown in Figure 1b. SEM shows that the most frequent issue with NPs is that all the samples are aggregated and lack any distinctive dopant-dependent morphological traits.[44] Nanoparticles have an increased relative surface area, a greater relative number of surface atoms, unsaturated coordination, and unoccupied coordinate sites on each atom. They attempt to create bonds, and, since these bonds often occur between particles close to one another, NPs clump together. Figure 1c shows the EDX spectra of Co (0.01):ZnS. The EDX results suggest that Co: Zn has an atomic ratio of 9:91, somewhat lower than the nominal ratio (Fig. 1c). Figure 1d displays the FTIR spectra of both the pure and codoped ZnS nanoparticles. The absorption bands at about 3499 cm^{-1} correspond to the O-H mode, while those at 2934 cm^{-1} correspond to the C-H mode. The peaks near 1400–1700 cm^{-1} correspond to the C = O stretching mode, the absorption peaks at 616 cm^{-1} indicate vibrations of Zn-S, the peaks at 616–1103 cm^{-1} are due to the connection between cobalt and sulfur, and the extra signal at 1386 cm^{-1} indicates Zn-S and Co-S bonding.

The sample's porosity and specific surface area have been studied using the BET characterization technique. Figure 2 compares the isotherm and pore size distribution collected for the pure and doped ZnS samples. The relative pressure (p/p_0) range of the N_2 adsorption–desorption isotherm hysteresis loop in all the samples is between 0.45 and 0.95. The obtained isotherm was compared with the IUPAC technical report for physisorption in solids and fine powders, and it is understood that all the samples have type IV isotherms with a mesoporous nature.[45] The pore size distribution also shows the existence of mesopores (2–50 nm) in the sample.[46] The BET surface area calculated from the isotherm for pure ZnS, Co (0.01):ZnS and Co (0.05):ZnS are 30.89, 73.20, and 99.30 $m^2\ g^{-1}$ respectively, indicating that the Co-doped ZnS material has an enhanced surface area compared to pure ZnS, which improves its electrochemical performance as a

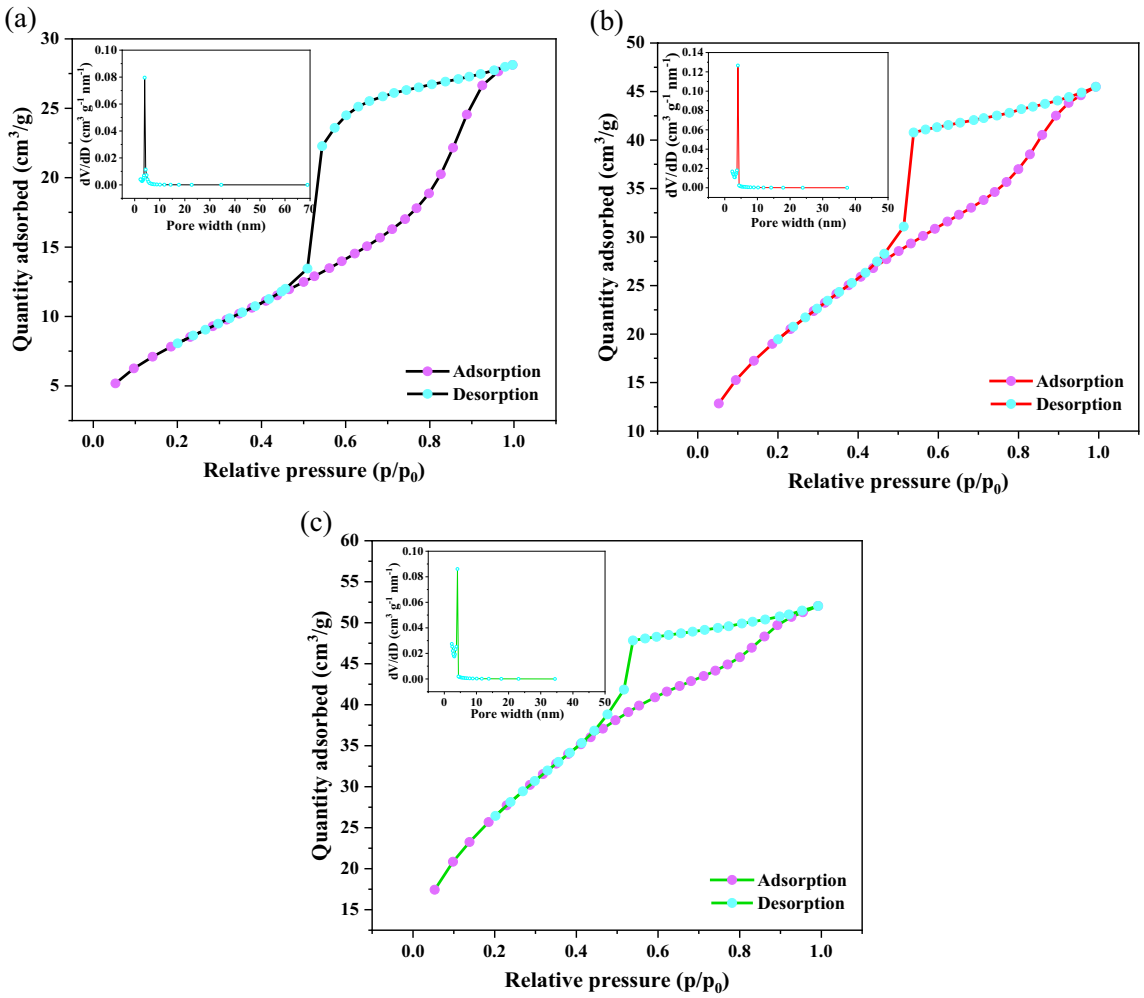

Fig. 2 BET analysis of pure and Co-doped ZnS samples with N2 adsorption–desorption isotherms: (a) ZnS, (b) Co (0.01):ZnS, (c) Co (0.05):ZnS; *inset* of each isotherm graph shows the corresponding pore size distribution of the sample.

supercapacitor.[46] The average pore diameter and pore volume comparison of the pure and doped ZnS samples are given in supplementary Table S2, which shows a reduction in pore size and an increase in total pore volume with Co-doping.

Electrochemical Measurements

A straightforward 3-electrode system setup was used for all electrochemical analyses of the undoped and doped ZnS samples. Different electrochemical characterization methods, including galvanostatic charge–discharge (GCD), cyclic voltammetry (CV), and EIS in a 3-M KOH electrolyte medium, were used to examine the behavior of the supercapacitor.

The specific capacitance values of the pure and doped ZnS samples were determined from the GCD curve at various current densities (Fig. 3). The specific capacitance was computed from GCD using:

$$C = \frac{(I/m) * t_d}{V} \tag{4}$$

where C is the specific capacitance (Fg^{-1}), I/m is the current density (Ag^{-1}), t_d is the discharging time (s), and V is the voltage window (V). The specific capacitance calculated from the GCD curve of pure ZnS, Co (0.01):ZnS, Co (0.03):ZnS, and Co (0.05):ZnS are 344.4 Fg^{-1}, 396.4 Fg^{-1}, 635.2 Fg^{-1}, and 606 Fg^{-1}, respectively, at 1 Ag^{-1}. The specific capacitance of samples decreases with increasing current density, which indicates the inaccessibility of inner electrochemical active sites at high current density.[47] From the GCD curves, specific capacity (Cg^{-1}) values of samples can be calculated by multiplying the specific capacitance (Fg^{-1}) value by the potential window FgCD (V). From the

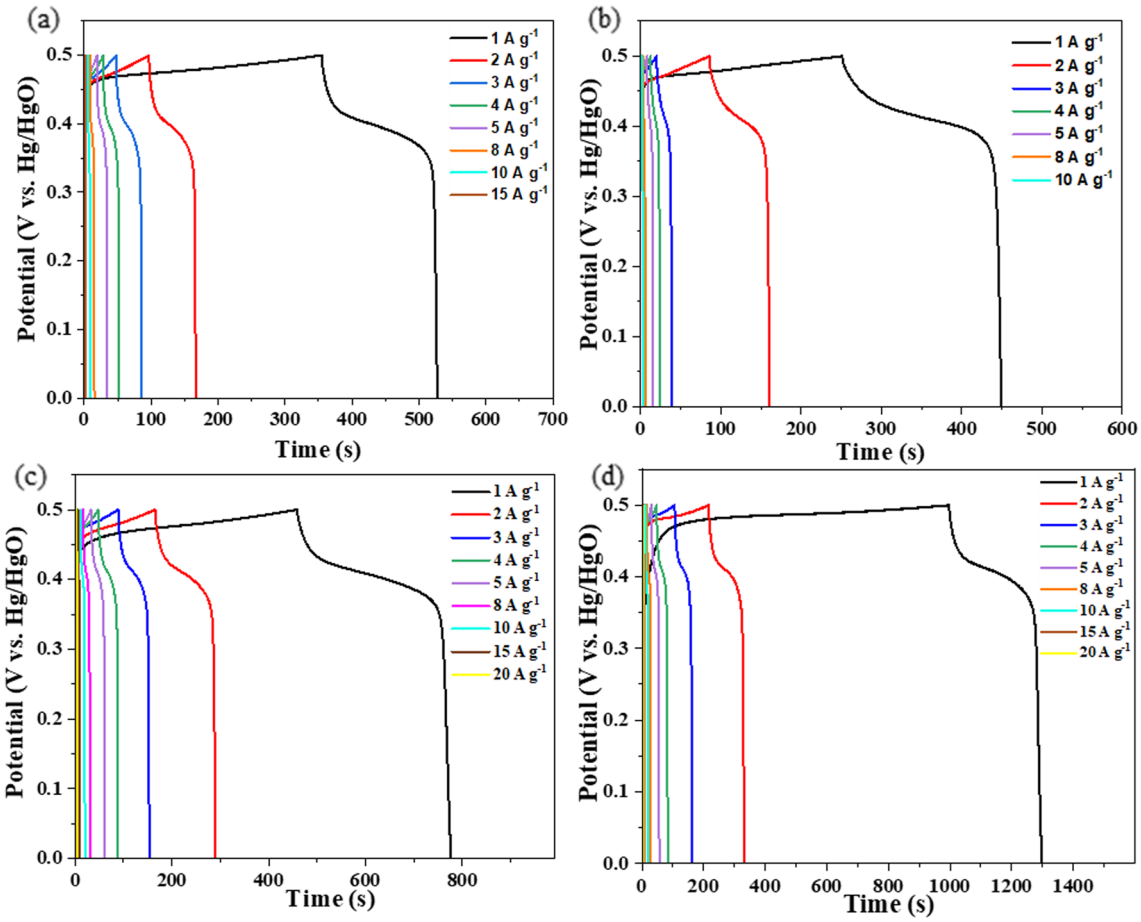

Fig. 3 Electrochemical charge–discharge curves taken at different current densities for (a) ZnS, (b) Co (0.01):ZnS, (c) Co (0.03):ZnS, (d) Co (0.05):ZnS, in the three-electrode system, using 3 M KOH electrolyte.

comparison plot of specific capacitance obtained through the GCD technique (supplementary Figure S1) for the pure and doped ZnS samples, it is clear that there is not much difference in the performance of Co (0.03):ZnS and Co (0.05):ZnS at all current densities, and the performance is better compared to pure ZnS.

Undoped and Co-doped samples are compared in Fig.4b using scan rates of 10 mV s^{-1}. The greater charge storage ability of the doped ZnS samples is indicated by a higher integral area under their CV curve compared to pure ZnS. The comparison of the GCD profile at 1 Ag^{-1}, as shown in Fig. 4a, also makes obvious the increased supercapacitive nature of the doped samples.

The potential window for the CV cycles is 0.1–0.65 V (vs. Hg/HgO) (for pure ZnS, it is 0.05–0.65 V) at various scan rates (5–100 mVs^{-1}). Figure 5 shows the specific capacitance of the pure and doped ZnS samples at various scan rates. The specific capacitance is highest at the lowest scan rate and declines as the scan rate is increased. Due to the rapid ion mobility, this may be connected to incomplete redox reactions occurring at high scan speeds. The mass transfer limitation of ions in electrolytes is caused, in part, by the inaccessibility of the inner side of the electroactive material (other than the surface) at higher scan speeds.[47] The specific capacitance can be calculated from the CV cycle using:

$$C = \frac{\int IdV}{2 * m * s * v} \tag{5}$$

where C is the specific capacitance (Fg^{-1}), $\int IdV$ is the integral area under the CV curve (A V), v is the potential window of the CV curve (V), s is the potential scan rate (Vs^{-1}), and m is the mass of electroactive material (g). From the CV at a scan rate of 10 mVs^{-1}, the specific capacitance of pure ZnS, Co (0.01):ZnS, Co (0.03):ZnS, and Co (0.05):ZnS are 460.7 Fg^{-1}, 721.6 Fg^{-1}, 867.5 Fg^{-1}, and 947.8 Fg^{-1}, respectively. At lower scan rates, the specific capacitance of samples follows the order Co (0.05):ZnS > Co (0.03):ZnS > Co (0.01):ZnS > ZnS (supplementary Figure S2). However, at higher scan rates, the specific capacitance order changes to Co (0.03):ZnS > Co (0.05):ZnS > Co (0.01):ZnS > ZnS. It

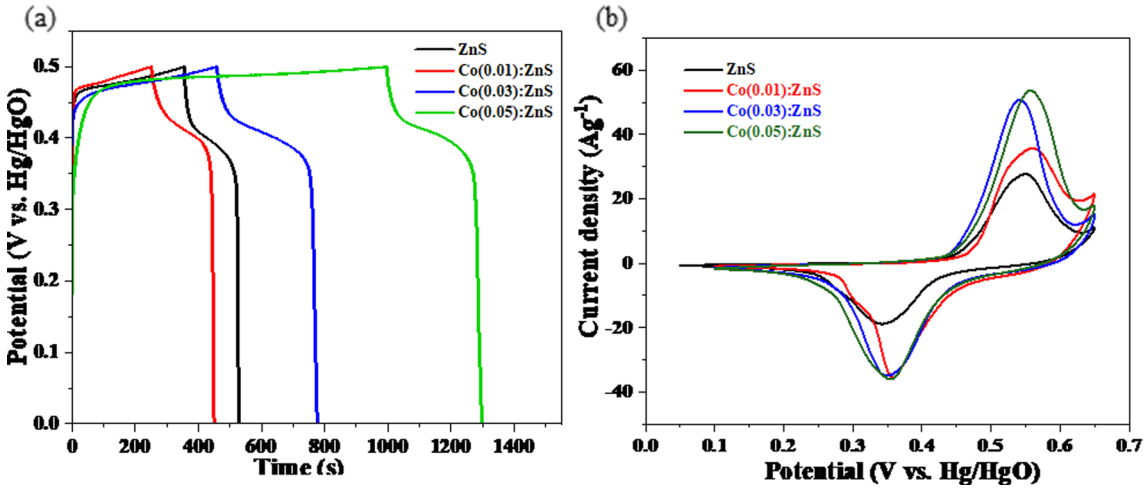

Fig. 4 Electrochemical performance comparison of pure and Co-doped ZnS: (a) charge–discharge curve comparison at the current density of 1 A g^{-1} , (b) CV curve comparison at a scan rate of 10 mV s^{-1} in the three-electrode system using 3 M KOH electrolyte.

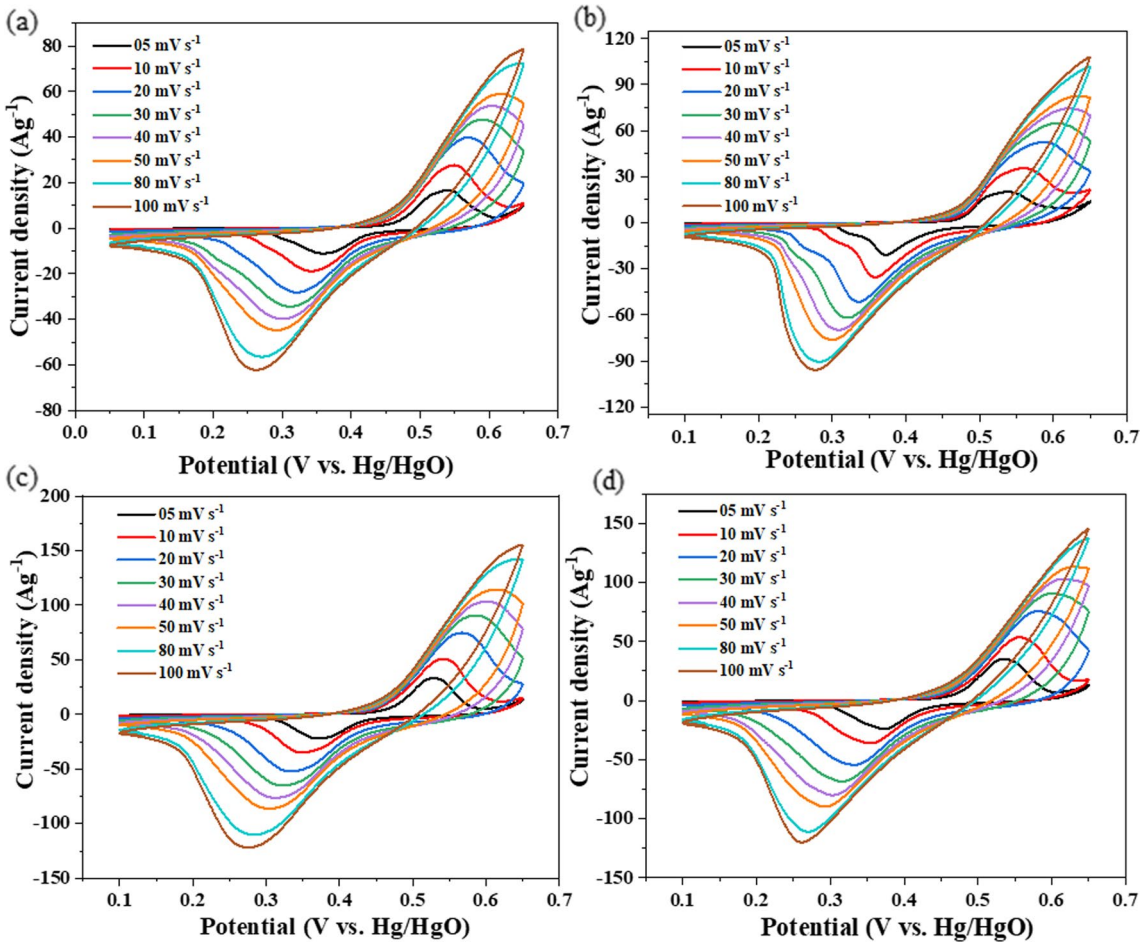

Fig. 5 Electrochemical cyclic voltammetry (CV) curves taken at different scan rates for (a) ZnS, (b) Co (0.01):ZnS, (c) Co (0.03):ZnS, (d) Co (0.05):ZnS, in the three-electrode system, using 3 M KOH electrolyte.

is clear from the specific capacitance measured during the CV cycle that adding a modest amount of Co dope enhances the super-capacitive characteristic of ZnS. The sample's particular capacity (Cg^{-1}) can be determined from the CV cycle by multiplying its specific capacitance (Fg^{-1}) by the CV cycle's associated potential window (V) (Fig. 6).

The potential window in GCD for the charge–discharging process is 0–0.5 V. The potential window in GCD was kept below 0.5 V to avoid the current generated through water electrolysis during the process. Compared to CV cycles in which the potential is varied, avoiding water electrolysis is crucial in GCD since the material has to achieve the fixed potential value.

EIS can be used to understand the kinetics of the electrodes. The comparison figure unmistakably demonstrates how doping with Co improved the kinetics of ZnS. The comparison (supplementary Table S4) that contains internal series resistance ®$_s$) and charge–transfer resistance ®$_{ct}$) of the pure and Co-doped samples (supplementary Table S3), as well as the equivalent circuits (supplementary Figure S3), are included in the supplemental information. The analogous circuit model also includes constant phase elements (Q_1 and $Q_{2)}$ and Warburg impedance, representing ion diffusion resistance due to ion transport from the electrolyte to the electrode surface. The R_s value, which takes into account the electrolyte's ionic conductivity, electrode contact resistance, and electroactive material intrinsic resistance, follows the order Co (0.05):ZnS < Co (0.03):ZnS < Co (0.01):ZnS < ZnS.[47] The dramatic drop in R_{ct} values brought on by the co-doping speeds up the redox reaction rate at the electrode surface.[10] The reduced interfacial R_{ct} value increases conductivity, leading to rapid electrochemical reactions at the surface and better energy storage.

The cyclic stability of the material was also tested by performing a GCD experiment at a current density of 2 Ag^{-1}. Supplementary Figure S4 indicates the capacitance retention (%) after 500 and 1000 cycles. The capacitance retention after 500 GCD cycles follows the order Co (0.03):ZnS < ZnS < Co (0.05):ZnS < Co (0.01):ZnS. The stability results are supported by the specific capacitance variation from GCD profiling (see supplementary Figure S1). The stability of the sample can be improved by co-doping with other atoms,[32,48] changing the morphology of the sample[47], and making a composite with carbon-based materials. [49,50] or other oxide/sulfide systems.[51–53] Incorporating EDLC with a pseudo-capacitive nature will make the system hybrid, boosting cyclic stability and electrochemical performance.[48]

Conclusions

Pure and co-doped ZnS powder samples were synthesized using a simple co-precipitation technique and their electrochemical performance has been studied. Co doping in ZnS enhances the specific capacitance to 947.8 Fg^{-1} for Co (0.05):ZnS which is only 460.7 Fg^{-1} for pure ZnS at a scan rate of 10 mVs^{-1}. Co-doping helps to improve the electrochemical performance in the following manner. First, co-doping in ZnS helps to increase the kinetics and rate of redox reactions by reducing R_{ct} values. Secondly, the enhancement in surface area due to Co incorporation into ZnS leads to an increase in electrochemical active sites, which supports the storage capacity of the sample. Finally, the Co doping in ZnS changes the sample's crystallite size, which ultimately contributes to the kinetics of charge transfer, fast faradaic reaction, and electrochemical performance. These promising results ensure the chances of improving the energy storage capacity of earth-abundant ZnS samples by elemental doping with other transition metal elements. The sudden improvement with simple Co doping opens up further possibilities of enhancement in performance by co-doping, in designing composite material, and in developing hybrid systems.

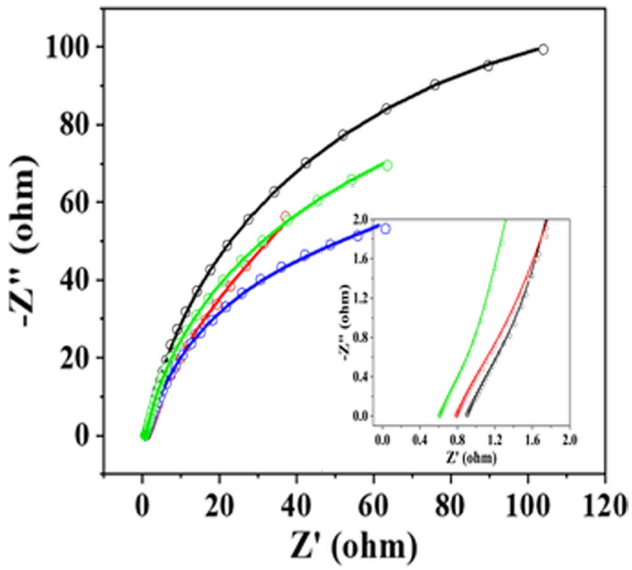

Fig. 6 Electrochemical Impedance analysis using Nyquist plots for pure (black) and Co-doped ZnS (red Co (0.01):ZnS, blue Co (0.03):ZnS, and green Co (0.05):ZnS) samples in a three-electrode system. Inset the magnified spectrum of high-frequency regions (circles collected data, and solid lines fitted curves) (Color figure online).

Supplementary Information The online version contains supplementary material available at https://doi.org/10.1007/s11664-024-11535-6.

Acknowledgments The authors acknowledge Ms. Sindhu Ramachandran (Department of Metallurgical and Materials Engineering, Indian Institute of Technology Madras, Chennai-600036, Tamil Nadu) for providing technical help during electrochemical measurements.

Funding Open Access funding provided by the Qatar National Library. Qatar National Research Fund supported this work under grant no.

MME03-1226-210042. The statements made herein are solely the responsibility of the authors.

Conflict of interest The authors have no competing interests to declare relevant to this article's content.

References

1. H. Yang, A Comparative Study of Supercapacitor Capacitance Characterization Methods. *Journal of Energy Storage* 29, 101316 (2020). https://doi.org/10.1016/j.est.2020.101316.
2. Bhoyate, S.; Kahol, P.; Gupta, R. Nanostructured Materials for Supercapacitor Applications; 2018; pp 1–29. https://doi.org/10.1039/9781788013871-00001.
3. M. Ashourdan, A. Semnani, F. Hasanpour, and S.E. Moosavifard, Synthesis of CuMnO2/Graphene Quantum Dot Nanocomposites as Novel Electrode Materials for High Performance Supercapacitors. *J. Energy Stor.* 36, 102449 (2021). https://doi.org/10.1016/j.est.2021.102449.
4. S. Verma, S. Arya, V. Gupta, S. Mahajan, H. Furukawa, and A. Khosla, Performance Analysis, Challenges and Future Perspectives of Nickel Based Nanostructured Electrodes for Electrochemical Supercapacitors. *J. Market. Res.* 11, 564–599 (2021). https://doi.org/10.1016/j.jmrt.2021.01.027.
5. X. Zhao, B.M. Sánchez, P.J. Dobson, and P.S. Grant, The Role of Nanomaterials in Redox-Based Supercapacitors for next Generation Energy Storage Devices. *Nanoscale* 3(3), 839–855 (2011). https://doi.org/10.1039/C0NR00594K.
6. Y. Zeng, M. Yu, Y. Meng, P. Fang, X. Lu, and Y. Tong, Iron-Based Supercapacitor Electrodes: Advances and Challenges. *Adv. Energy Mater.* 6(24), 1601053 (2016). https://doi.org/10.1002/aenm.201601053.
7. Z. Wang, W. Jia, M. Jiang, C. Chen, and Y. Li, One-Step Accurate Synthesis of Shell Controllable CoFe2O4 Hollow Microspheres as High-Performance Electrode Materials in Supercapacitor. *Nano Res.* 9(7), 2026–2033 (2016). https://doi.org/10.1007/s12274-016-1093-y.
8. A. Vlad, N. Singh, J. Rolland, S. Melinte, P.M. Ajayan, and J.-F. Gohy, Hybrid Supercapacitor-Battery Materials for Fast Electrochemical Charge Storage. *Sci. Rep.* 4(1), 4315 (2014). https://doi.org/10.1038/srep04315.
9. D. Gao, Z. Luo, C. Liu, and S. Fan, A Survey of Hybrid Energy Devices Based on Supercapacitors. *Green Energy & Environment* 8(4), 972–988 (2023). https://doi.org/10.1016/j.gee.2022.02.002.
10. Lukatskaya, M. R.; Kota, S.; Lin, Z.; Zhao, M. Q.; Shpigel, N.; Levi, M. D.; Halim, J.; Taberna, P. L.; Barsoum, M. W.; Simon, P.; Gogotsi, Y. Ultra-High-Rate Pseudocapacitive Energy Storage in Two-Dimensional Transition Metal Carbides. In *MXenes: From Discovery to Applications of Two-Dimensional Metal Carbides and Nitrides*; Jenny Stanford Publishing, 2023; pp 723–743.
11. A. Bharti Kumar, G. Ahmed, M. Gupta, P. Bocchetta, R. Adalati, R. Chandra, and Y. Kumar, Theories and Models of Supercapacitors with Recent Advancements: Impact and Interpretations. *Nano Ex.* 2(2), 022004 (2021). https://doi.org/10.1088/2632-959X/abf8c2.
12. I. Hussain, D. Mohapatra, G. Dhakal, C. Lamiel, S. Mohamed, M. Sayed, and J.-J. Shim, Different Controlled Nanostructures of Mn-Doped ZnS for High-Performance Supercapacitor Applications. *Journal of Energy Storage* 32, 101767 (2020). https://doi.org/10.1016/j.est.2020.101767.
13. M.S. Javed, C. Zhang, L. Chen, Y. Xi, and C. Hu, Hierarchical Mesoporous NiFe2O4 Nanocone Forest Directly Growing on Carbon Textile for High Performance Flexible Supercapacitors. *J. Mater. Chem. A* 4(22), 8851–8859 (2016). https://doi.org/10.1039/C6TA01893A.
14. J.H. Park, O.O. Park, K.H. Shin, C.S. Jin, and J.H. Kim, An Electrochemical Capacitor Based on a Ni(OH)2/Activated Carbon Composite Electrode. *Electrochem. Solid-State Lett.* 5(2), H7–H10 (2002). https://doi.org/10.1149/1.1432245.
15. J. Sung, and C. Shin, Recent Studies on Supercapacitors with Next-Generation Structures. *Micromachines* 11(12), 1125 (2020). https://doi.org/10.3390/mi11121125.
16. R. Ramya, R. Sivasubramanian, and M.V. Sangaranarayanan, Conducting Polymers-Based Electrochemical Supercapacitors—Progress and Prospects. *Electrochim. Acta* 101, 109–129 (2013). https://doi.org/10.1016/j.electacta.2012.09.116.
17. M.A.A. Mohd Abdah, N.H.N. Azman, S. Kulandaivalu, and Y. Sulaiman, Review of the Use of Transition-Metal-Oxide and Conducting Polymer-Based Fibres for High-Performance Supercapacitors. *Mater. Des.* 186, 108199 (2020). https://doi.org/10.1016/j.matdes.2019.108199.
18. Y. Zhou, W. Guo, and T. Li, A Review on Transition Metal Nitrides as Electrode Materials for Supercapacitors. *Ceram. Int.* 45(17), 21062–21076 (2019). https://doi.org/10.1016/j.ceramint.2019.07.151.
19. S. Ghosh, S.M. Jeong, and S.R. Polaki, A Review on Metal Nitride/Oxynitride as an Emerging Supercapacitor Electrode beyond Oxides. *Korean J. Chem. Eng.* 35, 1389–1408 (2018). https://doi.org/10.1007/s11814-018-0089-6.
20. Y. Gao and L. Zhao, Review on Recent Advances in Nanostructured Transition-Metal-Sulfide-Based Electrode Materials for Cathode Materials of Asymmetric Supercapacitors. *Chem. Eng. J.* 430, 132745 (2022). https://doi.org/10.1016/j.cej.2021.132745.
21. J. Rehman, K. Eid, R. Ali, X. Fan, G. Murtaza, M. Faizan, A. Laref, W. Zheng, and R.S. Varma, Engineering of Transition Metal Sulfide Nanostructures as Efficient Electrodes for High-Performance Supercapacitors. *ACS Appl. Energy Mater.* 5(6), 6481–6498 (2022). https://doi.org/10.1021/acsaem.1c03937.
22. I. Hussain, D. Mohapatra, G. Dhakal, C. Lamiel, M. Sayed, S. Sahoo, S. Mohamed, J. Kim, Y. Lee, and J.-J. Shim, Uniform Growth of ZnS Nanoflakes for High-Performance Supercapacitor Applications. *J. Energy Stor.* 36, 102408 (2021). https://doi.org/10.1016/j.est.2021.102408.
23. Y. Dahiya, M. Hariram, M. Kumar, T. Jain, and D. Sarkar, Modified Transition Metal Chalcogenides for High Performance Supercapacitors: Current Trends and Emerging Opportunities. *Coord. Chem. Rev.* 451, 214265 (2022). https://doi.org/10.1016/j.ccr.2021.214265.
24. P. Syedvali, G. Rajeshkhanna, E. Umeshbabu, G.U. Kiran, G.R. Rao, and P. Justin, In Situ Fabrication of Graphene Decorated Microstructured Globe Artichokes of Partial Molar Nickel Cobaltite Anchored on a Ni Foam as a High-Performance Supercapacitor Electrode. *RSC Adv.* 5(48), 38407–38416 (2015). https://doi.org/10.1039/C5RA03463A.

25. R. Liu, A. Zhou, X. Zhang, J. Mu, H. Che, Y. Wang, T. Wang, Z. Zhang, and Z. Kou, Fundamentals, Advances and Challenges of Transition Metal Compounds-Based Supercapacitors. *Chem. Eng. J.* 412, 128611 (2021). https://doi.org/10.1016/j.cej.2021.128611.
26. T.-F. Yi, Y. Li, Y.-M. Li, S. Luo, and Y.-G. Liu, ZnS Nanoparticles as the Electrode Materials for High-Performance Supercapacitors. *Solid State Ionics* 343, 115074 (2019). https://doi.org/10.1016/j.ssi.2019.115074.
27. I. Hussain, D. Mohapatra, G. Dhakal, C. Lamiel, M.S. Sayed, S. Sahoo, S.G. Mohamed, J.S. Kim, Y.R. Lee, and J.-J. Shim, Uniform Growth of ZnS Nanoflakes for High-Performance Supercapacitor Applications. *Journal of Energy Storage* 36, 102408 (2021). https://doi.org/10.1016/j.est.2021.102408.
28. M.W. Alam, H.S. Al Qahtani, H. Albalawi, M. Aamir, M. Bilal, T. Ahmad Mir, B. Souayeh, and N. Zaidi, Enhanced Electrodes for Supercapacitor Applications Prepared by Hydrothermal-Assisted Nano Sheet-Shaped MgCo2O4@ZnS. *Crystals* 12(6), 822 (2022). https://doi.org/10.3390/cryst12060822.
29. G. Rahman, W. Nawab, W. Zazai, S. Bilal, A.-H. Shah, and S. Mian, Exploring the Structural and Charge Storage Properties of Ni–ZnS/ZnO Composite Synthesized by One-Pot Wet Chemical Route. *Mater. Chem. Phys.* 252, 123203 (2020). https://doi.org/10.1016/j.matchemphys.2020.123203.
30. R. Rajendran, S. Murugan, P. Kollu, B. Raghupathy, S. Jeong, and A. Grace, Solvothermal Synthesis of Zinc Sulfide Decorated Graphene (ZnS/G) Nanocomposites for Novel Supercapacitor Electrodes. *Electrochim. Acta* (2015). https://doi.org/10.1016/j.electacta.2015.08.010.
31. M. Rauf, S.S. Shah, S. Shah, S.N.A. Shah, T. Haq, J. Shah, A. Ullah, T. Ahmad, Y. Khan, M. Aziz, and K. Hayat, Facile Hydrothermal Synthesis of Zinc Sulfide Nanowires for High-Performance Asymmetric Supercapacitor. *J. Saudi Chem. Soc.* 26, 101514 (2022). https://doi.org/10.1016/j.jscs.2022.101514.
32. A. Ali, D. Aadil, A. Rasheed, I. Hameed, S. Ajmal, I. Shakir, and M. Warsi, Honeycomb like Architectures of the Mo Doped ZnS@Ni for High-Performance Asymmetric Supercapacitors Applications. *Synth. Met.* 265, 116408 (2020). https://doi.org/10.1016/j.synthmet.2020.116408.
33. A. Rose, S. Balasubramanian, T. Maiyalagan, and T. Vijayakumar, Investigation on the Electrochemical Properties of Hydrothermally Synthesized Pure and Nickel Doped Zinc Sulfide Microspheres for Supercapacitor Electrode Applications. *J. Mater. Sci. Mater. Electron.* 27, 1–9 (2020). https://doi.org/10.1007/s10854-020-04456-7.
34. A. Jrad, M. Naouai, A. Abdallah, S. Ammar, and N. Turki-Kamoun, Doping ZnS Films with Cobalt: Structural, Compositional, Morphological, Optical, Electrical, Magnetic and Photocatalytic Properties. *Physica B* 603, 412776 (2021). https://doi.org/10.1016/j.physb.2020.412776.
35. M. Shobana and S.R. Meher, Effect of Cobalt Doping on the Structural, Optical and Magnetic Properties of Sol-Gel Derived ZnS Nanocrystalline Thin Films and Ab Initio Studies. *Thin Solid Films* 683, 97–110 (2019). https://doi.org/10.1016/j.tsf.2019.05.037.
36. R. Ashokkumar, K. Geetha, and P. Prabukanthan, Synthesis of Ni 2+ ions dopped zns nano particles by chemical precipitation method and their characterization. *J. Non-Oxide Glasses* 7, 13–21 (2015).
37. S. Basha, V. Khidhirbrahmendra, M. Jonnalagadda, U.S. Udayachandran Thampy, C. Reddy, and R.V.S.S.N. Ravikumar, Structural, Optical, Magnetic and Thermal Investigations on Cr3+ Ions Doped ZnS Nanocrystals by Co-Precipitation Method. *J. Sci. Adv. Mater. Dev.* (2019). https://doi.org/10.1016/j.jsamd.2019.03.002.
38. M. Moussaoui, R. Saoudi, A. Tishchenko, and F. Chassagneux, Tunable Optical Properties of ZnS Nanoparticles. *Electromagnetic and Light Scattering* 12, 178 (2010).
39. D.F. Fang, Z.M. Zhang, Z.P. Wang, and Z.J. Ding, Study of Photoluminescence of CdS/ZnS Core/Shell Quantum Dots. *Phys. Procedia* 32, 920–925 (2012). https://doi.org/10.1016/j.phpro.2012.03.657.
40. J.K. Salem, T.M. Hammad, S. Kuhn, M.A. Draaz, N.K. Hejazy, and R. Hempelmann, Structural and Optical Properties of Co-Doped ZnS Nanoparticles Synthesized by a Capping Agent. *J. Mater. Sci. Mater. Electron.* 25(5), 2177–2182 (2014). https://doi.org/10.1007/s10854-014-1856-8.
41. C. Bi, L. Pan, M. Xu, J. Yin, L. Qin, J. Liu, H. Zhu, and J.Q. Xiao, Synthesis and Characterization of Co-Doped Wurtzite ZnS Nanocrystals. *Mater. Chem. Phys.* 116(2), 363–367 (2009). https://doi.org/10.1016/j.matchemphys.2009.03.037.
42. B. Poornaprakash, D. Amaranatha Reddy, G. Murali, N. Madhusudhana Rao, R.P. Vijayalakshmi, and B.K. Reddy, Composition Dependent Room Temperature Ferromagnetism and PL Intensity of Cobalt Doped ZnS Nanoparticles. *J. Alloy. Compd.* 577, 79–85 (2013). https://doi.org/10.1016/j.jallcom.2013.04.106.
43. B. Poornaprakash, U. Chalapathi, P. Poojitha, and S. Vattikuti, Co-Doped ZnS Quantum Dots: Structural, Optical, Photoluminescence, Magnetic, and Photocatalytic Properties. *J. Supercond. Novel Magn.* (2020). https://doi.org/10.1007/s10948-019-05223-4.
44. B. Poornaprakash, U. Chalapathi, and S. Vattikuti, Compositional, Morphological, Structural, Microstructural, Optical, and Magnetic Properties of Fe Co, and Ni Doped ZnS Nanoparticles. *Appl. Phys. A* (2017). https://doi.org/10.1007/s00339-017-0865-x.
45. M. Thommes, K. Kaneko, A.V. Neimark, J.P. Olivier, F. Rodriguez-Reinoso, J. Rouquerol, and K.S.W. Sing, Physisorption of Gases, with Special Reference to the Evaluation of Surface Area and Pore Size Distribution (IUPAC Technical Report). *Pure Appl. Chem.* 87(9–10), 1051–1069 (2015). https://doi.org/10.1515/pac-2014-1117.
46. A. Manalu, K. Tarigan, S. Humaidi, M. Ginting, and I.P. Manalu, Effect of Surface Area on Electrical Properties of NiCo2O4-Reduced Graphene Oxide Nanocomposites for Supercapacitor Electrodes Applications. *MSET* 5(1), 444–451 (2022). https://doi.org/10.1016/j.mset.2022.10.004.
47. G.S. Kaliaraj and A. Ramadoss, Nickel-Zinc Sulfide Nanocomposite Thin Film as an Efficient Cathode Material for High-Performance Hybrid Supercapacitors. *Mater. Sci. Semicond. Process.* 105, 104709 (2020). https://doi.org/10.1016/j.mssp.2019.104709.
48. Z. Li, J. Lin, B. Li, C. Yu, H. Wang, and Q. Li, Construction of Heteroatom-Doped and Three-Dimensional Graphene Materials for the Applications in Supercapacitors: A Review. *Journal of Energy Storage* 44, 103437 (2021). https://doi.org/10.1016/j.est.2021.103437.
49. M. Jing, Z. Chen, Z. Li, F. Li, M. Chen, M. Zhou, B. He, L. Chen, Z. Hou, and X. Chen, Facile Synthesis of ZnS/N, S Co-Doped Carbon Composite from Zinc Metal Complex for High-Performance Sodium-Ion Batteries. *ACS Appl. Mater. Interfaces* 10(1), 704–712 (2018). https://doi.org/10.1021/acsami.7b15659.
50. R. Kumar, H.-J. Kim, S. Park, A. Srivastava, and I.-K. Oh, Graphene-Wrapped and Cobalt Oxide-Intercalated Hybrid for Extremely Durable Super-Capacitor with Ultrahigh Energy and Power Densities. *Carbon* 79, 192–202 (2014). https://doi.org/10.1016/j.carbon.2014.07.059.
51. M.S. Javed, T. Najam, M. Sajjad, S.S.A. Shah, I. Hussain, M. Idrees, M. Imran, M.A. Assiri, and S.H. Siyal, Design and Fabrication of Highly Porous 2D Bimetallic Sulfide ZnS/FeS Composite Nanosheets as an Advanced Negative Electrode Material for Supercapacitors. *Energy Fuels* 35(18), 15185–15191 (2021). https://doi.org/10.1021/acs.energyfuels.1c02444.
52. K.D. Ikkurthi, S.S. Rao, J.-W. Ahn, C.D. Sunesh, and H.-J. Kim, A Cabbage Leaf like Nanostructure of a NiS@ZnS Composite on Ni Foam with Excellent Electrochemical Performance for

Supercapacitors. *Dalton Trans.* 48(2), 578–586 (2019). https://doi.org/10.1039/C8DT04139C.

53. B. Wei, H. Liang, R. Wang, D. Zhang, Z. Qi, and Z. Wang, One-Step Synthesis of Graphitic-C3N4/ZnS Composites for Enhanced Supercapacitor Performance. *J. Energy Chem.* 27(2), 472–477 (2018). https://doi.org/10.1016/j.jechem.2017.11.015.